Journal of Alloys and Compounds 509 (2011) 7572–7578

Contents lists available at ScienceDirect

Journal of Alloys and Compounds

journal homepage: www.elsevier.com/locate/jallcom

The synergistic ability of Al_2O_3 nanoparticles to enhance mechanical response of hybrid alloy AZ31/AZ91

M. Paramsothy[a], J. Chan[b], R. Kwok[b], M. Gupta[a,*]

[a] Department of Mechanical Engineering, National University of Singapore, 9 Engineering Drive 1, Singapore 117576, Singapore
[b] Singapore Technologies Kinetics Ltd (ST Kinetics), 249 Jalan Boon Lay, Singapore 619523, Singapore

ARTICLE INFO

Article history:
Received 7 January 2011
Received in revised form 21 April 2011
Accepted 22 April 2011
Available online 30 April 2011

Keywords:
Hybrid alloy
AZ31/AZ91 nanocomposite
Al_2O_3 nanoparticle
Microstructure
Mechanical properties

ABSTRACT

AZ31/AZ91 hybrid alloy nanocomposite containing Al_2O_3 nanoparticle reinforcement was fabricated using solidification processing followed by hot extrusion. The nanocomposite exhibited similar grain size to the monolithic hybrid alloy, reasonable Al_2O_3 nanoparticle distribution, non-dominant (0002) texture in the longitudinal direction, and 25% higher hardness than the monolithic hybrid alloy. Compared to the monolithic hybrid alloy (in tension), the nanocomposite synergistically exhibited higher 0.2%TYS, UTS, failure strain and work of fracture (WOF) (+12%, +7%, +99% and +108%, respectively). Compared to the monolithic hybrid alloy (in compression), the nanocomposite exhibited higher 0.2%CYS and UCS, and lower failure strain and WOF (+5%, +3%, −7% and −7%, respectively). The beneficial effects of Al_2O_3 nanoparticle addition on the enhancement of tensile and compressive properties of AZ31/AZ91 hybrid alloy are investigated in this paper.

1. Introduction

The AZ series of magnesium alloys are commonly used in the world today. These alloys are characterized by: (a) low cost, (b) ease of handling, (c) good strength and ductility and (d) resistance to atmospheric corrosion. Using the friction stir processing technique, AZ31 has been surface-reinforced with SiC microparticulates [1], C_{60} molecules [2], and multi-walled carbon nanotubes [3]. Here, it was reported that particle dispersion was good and hardening of the base matrix at the surface occurred. Similar findings along with grain refinement were also reported for AZ31 reinforced with SiC and B_4C microparticulates using gas-tungsten arc (GTA) with simultaneous reinforcement powder feeding processing technique [4–6]. In this case regarding AZ31/SiC microcomposite, defect-free and adherent particle–matrix interface has been reported [5,6]. In the case of AZ61, yttrium has been added to increase dry oxidation resistance [7]. The alloy consisted of well-distributed fine circular phase depending on the choice of solidification processing parameters used (stirring temperature, velocity and time) [7]. SiO_2 nanoparticles have been added to AZ61 using friction stir processing [8]. Here, the tensile elongation at 350 °C of selected composites reached 350% at 1×10^{-2} s^{-1} and 420% at 1×10^{-1} s^{-1}. This implied that the dispersion of the SiO_2 nanoparticles was sufficiently uniform to clearly exhibit high strain rate super-plasticity (HSRSP) [8]. On the other hand, the tensile elongation at the same temperature at a lower strain rate of 1×10^{-3} s^{-1} was barely 100% [8]. SiC microparticles have also been added to AZ91 [9]. In this reported work, an increase in work hardening rate in the as-extruded composite during tensile deformation at room temperature was caused by grain refinement and uniform particle distribution. The uniaxial compressive deformation behavior of AZ91/SiC microcomposite has been investigated at elevated temperature (250–400 °C) [10]. The effective stress dependence on strain rate and temperature gave a stress exponent of $n = 5$ and a true activation energy of $Q = 99$ kJ/kmol [10]. This Q value was close to that of grain boundary diffusion in Mg and it was concluded that dislocation climb controlled the elevated temperature compressive deformation [10]. Multiple layer microcomposites consisting of alternating layers of: (a) AZ91 coated P100 pitch based fibers and (b) AZ61 foil have also been studied [11]. The reaction zone containing single and/or mixed metal carbides grew due to thermal treatment [11]. Technically, AZ31 may be alloyed with more pure aluminium to obtain the other more concentrated magnesium alloys in the AZ series. However, the mixing of two or more AZ series magnesium alloys for the same purpose (and consequent formation of a hybrid magnesium alloy) has not been reported. There may be certain advantages in this approach based on the: (a) lower liquidus temperature and (b) lower melt density (during stirring/mixing) of the AZ series magnesium alloys compared to pure aluminium. This means that in the hybrid alloy approach, the: (1) melting of alloys is completed at a lower temperature than the melting point of pure aluminium and (2) heterogenous nature of the molten alloys is significantly less

* Corresponding author. Tel.: +65 6516 6358; fax: +65 6779 1459.
E-mail address: mpegm@nus.edu.sg (M. Gupta).

0925-8388/$ – see front matter © 2011 Elsevier B.V. All rights reserved.
doi:10.1016/j.jallcom.2011.04.120

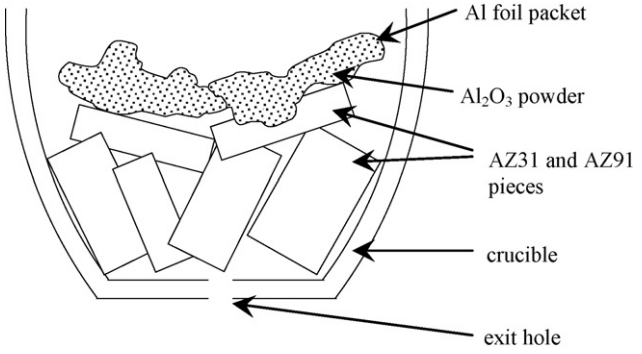

Fig. 1. Arrangement of raw materials in crucible before casting for AZ31/AZ91/Al_2O_3 nanocomposite.

before stirring/mixing compared to when pure aluminium is used. Open literature search has revealed that no successful attempt has been made to simultaneously increase tensile strength and ductility of AZ31/AZ91 hybrid magnesium alloy with Al_2O_3 or any other nanoparticles, using a high volume production spray-deposition based solidification processing technique.

Accordingly, one of the primary aims of this study was to synergistically simultaneously increase tensile strength and ductility of AZ31/AZ91 hybrid magnesium alloy with Al_2O_3 nanoparticles. Another aim of the present study was to evaluate the compressive properties of AZ31/AZ91/Al_2O_3 hybrid alloy nanocomposite. Disintegrated melt deposition (DMD) [12,13] followed by hot extrusion was used to synthesize the AZ31/AZ91/Al_2O_3 hybrid alloy nanocomposite.

2. Experimental procedures

2.1. Materials

In this study, AZ31 (nominally 2.50–3.50 wt.% Al, 0.60–1.40 wt.% Zn, 0.15–0.40 wt.% Mn, 0.10 wt.% Si, 0.05 wt.% Cu, 0.01 wt.% Fe, 0.01 wt.% Ni, balance Mg), and AZ91 (nominally 8.30–9.70 wt.% Al, 0.35–1.00 wt.% Zn, 0.15–0.50 wt.% Mn, 0.10 wt.% Si, 0.030 wt.% Cu, 0.005 wt.% Fe, 0.002 wt.% Ni, 0.02 wt.% others, balance Mg), both alloys supplied by Tokyo Magnesium Co. Ltd. (Yokohama, Japan), were used as matrix material. Equal masses of AZ31 and AZ91 were mixed to metallurgically upgrade AZ31. The intention of this mixing was to increase the nominal aluminium content of AZ31 by 3 wt.%. AZ31 and AZ91 blocks were sectioned to smaller pieces. All oxide and scale surfaces were removed using machining. All surfaces were washed with ethanol after machining. Al_2O_3 nanoparticles (50 nm size) supplied by Baikowski (Japan) was used as the reinforcement phase.

2.2. Processing

Monolithic AZ31/AZ91 hybrid alloy (nominal aluminium content of AZ31 increased by 3 wt.%) was cast using the DMD method [12,13]. This involved heating AZ31 and AZ91 blocks to 750 °C in an inert Ar gas atmosphere in a graphite crucible using a resistance heating furnace. The crucible was equipped with an arrangement for bottom pouring. Upon reaching the superheat temperature, the molten slurry was stirred for 2.5 min at 460 rpm using a twin blade (pitch 45°) mild steel impeller to facilitate the uniform distribution of heat. The impeller was coated with Zirtex 25 (86%ZrO_2, 8.8%Y_2O_3, 3.6%SiO_2, 1.2%K_2O and Na_2O, and 0.3% trace inorganics) to avoid iron contamination of the molten metal. The melt was then released through a 10 mm diameter orifice at the base of the crucible. The melt was disintegrated by two jets of argon gas oriented normal to the melt stream located 265 mm from the melt pouring point. The argon gas flow rate was maintained at 25 lpm. The disintegrated melt slurry was subsequently deposited onto a metallic substrate located 500 mm from the disintegration point. An ingot of 40 mm diameter was obtained following the deposition stage. To form the AZ31/AZ91/1.5 vol%Al_2O_3 hybrid alloy nanocomposite, Al_2O_3 nanoparticle powder was isolated by wrapping in Al foil of minimal weight (<0.50 wt.% with respect to AZ31 and AZ91 total matrix weight) and arranged on top of the AZ31 and AZ91 alloy blocks (see Fig. 1), with all other DMD parameters unchanged. All billets were machined to 35 mm diameter and hot extruded using 20.25:1 extrusion ratio on a 150 ton hydraulic press. The extrusion temperature was 350 °C. The billets were held at 400 °C for 60 min in a furnace prior to extrusion. Colloidal graphite was used as a lubricant. Rods of 8 mm were obtained.

2.3. Heat treatment

Heat treatment was carried out on all extruded sections at 200 °C for 1 h using a resistance heating furnace. This selection of temperature and time was made in order to relax the monolithic AZ31/AZ91 hybrid alloy (nominal aluminium content of AZ31 increased by 3 wt.%) without recrystallization softening. The recrystallization temperature of AZ61 magnesium alloy (as the nearest matching alloy in terms of composition) following 20% cold work after 1 h is 288 °C [14]). Prior to heat treatment, the sections were coated with colloidal graphite and wrapped in aluminium foil to minimize reaction with oxygen present in the furnace atmosphere.

2.4. Microstructural characterization

Microstructural characterization studies were conducted on metallographically polished monolithic and nanocomposite extruded samples to determine grain characteristics as well as nanoparticle reinforcement distribution. Hitachi S4300 Field-Emission SEM was used. Image analysis using Scion software was carried out to determine the grain characteristics. XRD studies were conducted using CuKα radiation (λ = 1.5406 Å) with a scan speed of 2°/min in an automated Shimadzu LAB-X XRD-6000 diffractometer to determine intermetallic phase(s) presence and dominant textures in the transverse and longitudinal (extrusion) directions.

2.5. Hardness

Microhardness measurements were made on polished monolithic and nanocomposite extruded samples. Vickers microhardness was measured with an automatic digital Shimadzu HMV Microhardness Tester using 25 gf-indenting load and 15 s dwell time.

2.6. Tensile testing

Smooth bar tensile properties of the monolithic and nanocomposite extruded samples were determined based on ASTM E8M-05. Round tension test samples of 5 mm diameter and 25 mm gauge length were subjected to tension using an MTS 810 machine equipped with an axial extensometer with a crosshead speed set at 0.254 mm/min. Fractography was performed on the tensile fracture surfaces using Hitachi S4300 FESEM.

2.7. Compressive testing

Compressive properties of the monolithic and nanocomposite extruded samples were determined based on ASTM E9-89a. Samples of 8 mm length (l) and 8 mm diameter (d) where $l/d = 1$ were subjected to compression using a MTS 810 machine with 0.005 min^{-1} strain rate. Fractography was performed on the compressive fracture surfaces using Hitachi S4300 FESEM.

3. Results

3.1. Macrostructural characteristics

No macropores or shrinkage cavities were observed in the cast monolithic and nanocomposite materials. No macrostructural defects were observed for extruded rods of monolithic and nanocomposite materials.

3.2. Microstructural characteristics

Microstructural analysis results revealed that grain size and aspect ratio remained statistically unchanged in the case of nanocomposite as shown in Table 1 and Fig. 2a and b. Al_2O_3 nanoparticle reinforcement and intermetallic particle distributions in the nanocomposite were overlapping each other and reasonably uniform as shown in Fig. 2c and d.

Texture results are listed in Table 2 and shown in Fig. 3. In monolithic and nanocomposite materials, the dominant texture in the transverse and longitudinal directions was (1 0 −1 1).

3.3. Hardness

The results of microhardness measurements are listed in Table 1. The nanocomposite exhibited higher hardness than the monolithic material.

Table 1
Results of grain characteristics and microhardness of AZ31/AZ91 and AZ31/AZ91/Al_2O_3 nanocomposite.

Material	Al_2O_3 (vol%)	Grain characteristics[a]		Microhardness (HV)
		Size (μm)	Aspect ratio	
AZ31/AZ91	–	5.1 ± 0.7	1.4	111 ± 5
AZ31/AZ91/1.5 vol%Al_2O_3	1.50	4.8 ± 1.0	1.4	139 ± 8 (+25)

( ) Brackets indicate % change with respect to corresponding result of AZ31/AZ91.
[a] Based on approximately 100 grains.

Table 2
Texture results of AZ31/AZ91 and AZ31/AZ91/Al_2O_3 nanocomposite based on X-ray diffraction.

Material	Section[a]	Plane	Average I/I_{max}[b]
AZ31/AZ91			
		1 0 −1 0 prism	0.53
	T	0 0 0 2 basal	0.26
		1 0 −1 1 pyramidal	**1.00**
		1 0 −1 0 prism	0.33
	L	0 0 0 2 basal	0.63
		1 0 −1 1 pyramidal	**1.00**
AZ31/AZ91/1.5 vol%Al_2O_3			
		1 0 −1 0 prism	0.49
	T	0 0 0 2 basal	0.22
		1 0 −1 1 pyramidal	**1.00**
		1 0 −1 0 prism	0.33
	L	0 0 0 2 basal	0.66
		1 0 −1 1 pyramidal	**1.00**

The bold values indicate the dominant texture in each section.
[a] T: transverse, L: longitudinal.
[b] I_{max} is XRD maximum intensity from either prism, basal or pyramidal planes.

3.4. Tensile behavior

The overall results of ambient temperature tensile testing of the extruded materials are shown in Table 3 and Fig. 4a. The strength, failure strain and work of fracture (WOF) of AZ31/AZ91/1.5 vol%Al_2O_3 were higher compared to monolithic AZ31/AZ91. The WOF was determined by computing the area under the stress–strain curve up to the point of fracture. The fractured surface of all extruded materials exhibited mixed (ductile + brittle) mode of fracture as shown in Fig. 5a and b.

3.5. Compressive behavior

The overall results of ambient temperature compressive testing of the extruded materials are shown in Table 4 and Fig. 4b. The strength of AZ31/AZ91/1.5 vol%Al_2O_3 was higher compared to monolithic AZ31/AZ91. Failure strain and WOF of AZ31/AZ91/1.5 vol%Al_2O_3 were lower than that of monolithic AZ31/AZ91. The fractured surface of AZ31/AZ91/1.5 vol%Al_2O_3 and monolithic AZ31/AZ91 appeared similarly rough as shown in Fig. 5c.

4. Discussion

4.1. Synthesis of monolithic AZ31/AZ91 and AZ31/AZ91/Al_2O_3 nanocomposite

Synthesis of monolithic and nanocomposite materials, the final form being extruded rods, was successfully accomplished with: (a) no detectable metal oxidation and (b) no detectable reaction

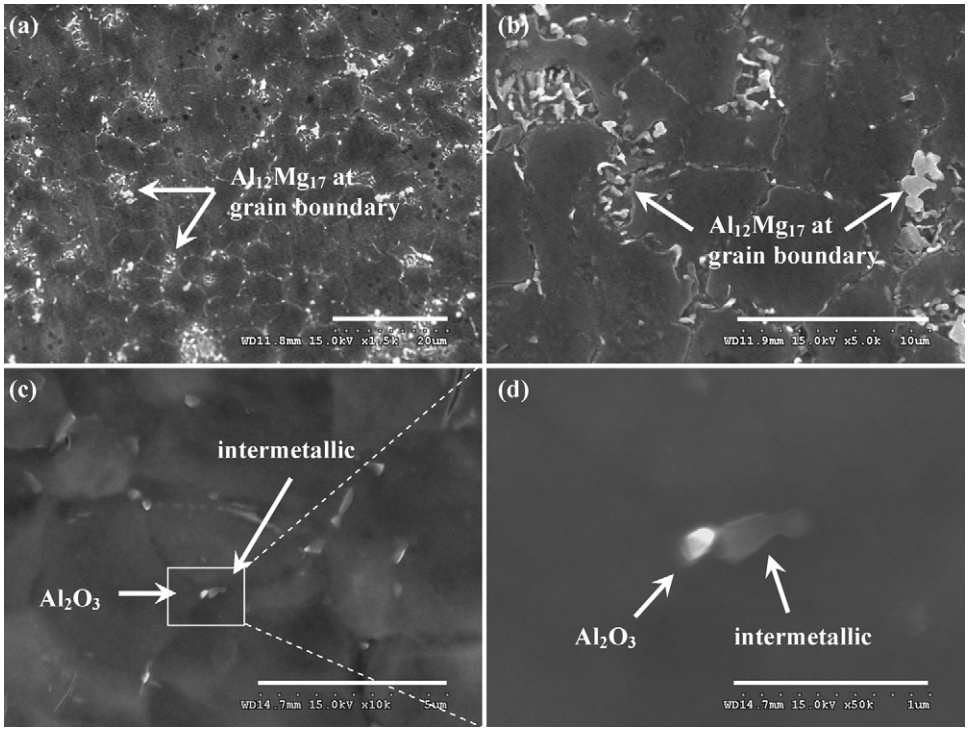

Fig. 2. Representative micrographs showing grain size in monolithic AZ31/AZ91 and AZ31/AZ91/Al_2O_3 nanocomposite: (a) lower magnification and (b) higher magnification. Representative micrographs showing the presence of individual Al_2O_3 nanoparticles and fine intermetallic particles in the AZ31/AZ91/Al_2O_3 nanocomposite: (c) lower magnification and (d) higher magnification.

Table 3
Results of tensile testing of AZ31/AZ91 and AZ31/AZ91/Al_2O_3 nanocomposite.

Material	0.2%TYS (MPa)	UTS (MPa)	Failure strain/elongation (%)	WOF (MJ/m^3)[a]
AZ31/AZ91	207 ± 4	316 ± 6	8.0 ± 0.1	24 ± 0
AZ31/AZ91/1.5 vol%Al_2O_3	232 ± 13 (+12)	339 ± 10 (+7)	15.9 ± 0.5 (+99)	50 ± 3 (+108)
Extruded AZ31B/C-F [14]	200	255	12	–
Extruded AZ61A-F [14]	205	305	16	–
Extruded AZ91D[b,c] [29,30]	215	296	10.2	–
Extruded AZ91D[b,d] [30]	226	313	15.6	–
Extruded ZK21A-F [14]	195	260	4	–
Extruded ZK31-T5 [14]	210	295	7	–
Extruded ZK40A-T5 [14]	255	275	4	–
Sand cast AZ63A-T6 [14]	130	275	5	–
Sand cast AZ81A-T4 [14]	83	275	15	–
Sand cast AZ91C/E-T6 [14]	145	275	6	–
Sand cast AZ92A-T6 [14]	150	275	3	–
Sand cast ZK61A-T5 [14]	185	310	–	–
Sand cast ZK61A-T6 [14]	195	310	10	–
Extruded Mg/0.22 vol% Y_2O_3[b,e] [31]	218 ± 2	277 ± 5	12.7 ± 1.3	29.6 ± 3.5
Extruded Mg/0.66 vol% Y_2O_3[b,e] [31]	312 ± 4	318 ± 2	6.9 ± 1.6	18.2 ± 4.7
Extruded Mg/1.11 vol% Al_2O_3[b,e] [28]	175 ± 3	246 ± 3	14.0 ± 2.4	31.7 ± 6.3
Extruded AZ91D/15 vol%SiCp[b,c,f] [29]	257	289	0.7	–
Extruded AZ91D/15 vol%SiCp[b,d,f] [29]	205	233	1.1	–

( ) Brackets indicate %change with respect to corresponding result of AZ31/AZ91.
[a] Obtained from engineering stress–strain diagram using EXCEL software.
[b] Hot extruded at 250 °C.
[c] Rheocast material prior to extrusion.
[d] Die-cast material prior to extrusion.
[e] Nano-size reinforcement.
[f] Micro-size reinforcement.

between graphite crucible and melts. The inert atmosphere used during DMD was effective in preventing oxidation of the Mg melt. No stable carbides of Mg or Al formed due to reaction with graphite crucible.

4.2. Microstructural characteristics

Microstructural characterization of extruded samples is discussed in terms of: (a) grain characteristics and (b) Al_2O_3 nanoparticle reinforcement distribution.

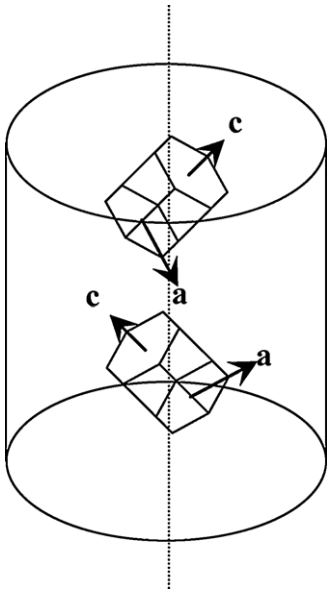

Fig. 3. Schematic diagram showing textures of monolithic AZ31/AZ91 and AZ31/AZ91/Al_2O_3 nanocomposite based on X-ray diffraction. In each case, vertical axis (dotted line) is parallel to extrusion direction. Each cell is made up of 2 HCP units having 1 common (0 0 0 2) basal plane.

Nearly equiaxed grains were observed in monolithic material and nanocomposite as shown in Table 1 and Fig. 2a and b. Grain size was statistically insignificant in the case of nanocomposite, suggesting the inability of Al_2O_3 nanoparticle to serve as either nucleation sites or obstacles to grain growth during solid state cooling. It was observed that β-$Al_{12}Mg_{17}$ intermetallic particles decorated the grain boundaries in the monolithic material and nanocomposite. X-ray diffraction (XRD) analysis revealed the presence of β-$Al_{12}Mg_{17}$ phase [15]).

The reasonably uniform distribution of Al_2O_3 nanoparticles as shown in Fig. 2c and d can be attributed to: (a) minimal gravity-associated segregation due to judicious selection of stirring parameters [12], (b) good wetting of Al_2O_3 nanoparticles by the alloy matrix [16–19], (c) argon gas disintegration of metallic stream [20], and (d) dynamic deposition of composite slurry on substrate followed by hot extrusion. Similar reasonably uniform distribution of Al_2O_3 nanoparticles in magnesium alloy AZ31 has also been recently reported [19]. In the nanocomposite, no reaction products based on Mg and Al_2O_3 (such as MgO in this case [21]) having more than 2% by volume were detected using X-ray diffraction analysis.

4.3. Mechanical behavior

4.3.1. Hardness

A significant increase in microhardness by 25% was observed in the nanocomposite when compared to monolithic material as listed in Table 1. This was consistent with earlier observations made on Mg/Al_2O_3, AZ31/C_{60} and AZ31/MWCNT nanocomposites [21–23]. The increase in hardness of the nanocomposite in the present study can be attributed to: (a) reasonably uniform distribution of harder Al_2O_3 nanoparticles in the matrix and (b) higher constraint to localized matrix deformation during indentation due to the presence of nanoparticles [21,22,24].

4.3.2. Tensile and compressive behavior

4.3.2.1. Strength. The tensile and compressive strengths of monolithic material and nanocomposite are listed in Tables 3 and 4

Table 4
Results of compressive testing of AZ31/AZ91 and AZ31/AZ91/Al_2O_3 nanocomposite.

Material	0.2%CYS (MPa)	UCS (MPa)	Failure strain/ductility (%)	WOF (MJ/m^3)[a]
AZ31/AZ91	117 ± 15	495 ± 13	19.6 ± 1.9	82 ± 6
AZ31/AZ91/1.5 vol%Al_2O_3	123 ± 16 (+5)	512 ± 3 (+3)	18.2 ± 0.7 (−7)	76 ± 4 (−7)
Extruded AZ31B/C-F [14]	97	–	–	–
Extruded AZ61A-F [14]	130	–	–	–
Sand cast AZ63A-T6 [14]	130	–	–	–
Sand cast AZ81A-T4 [14]	83	–	–	–
Sand cast HK31A-T6 [14]	105	–	–	–
Squeeze cast RZ5[b] [32]	–	308	16.7	–
Melt infiltrated RZ5/22 vol%Saffil[c] [32]	–	445	5.2	–

() Brackets indicate %change with respect to corresponding result of AZ31/AZ91.
[a] Obtained from engineering stress–strain diagram using EXCEL software.
[b] RZ5 has nominal composition of 4.2 wt.%Zn, 0.35 wt.%Zr, 1.3 wt.%RE (rare earth metals), balance Mg.
[c] Saffil (ICI tradename) has nominal dimensions of 3 μm diameter and 150 μm length, and approximate composition of 5 wt.%silica and balance δ-alumina.

(and shown in Fig. 4a and b), respectively. 0.2%TYS and UTS were enhanced by 12% and 7%, respectively, in AZ31/AZ91/1.5 vol%Al_2O_3 compared to monolithic material. In comparison of compressive strengths, 0.2%CYS and UCS of AZ31/AZ91/1.5 vol%Al_2O_3 were higher by 5% and 3%, respectively, compared to monolithic AZ31/AZ91. The stress detected at almost any given strain was higher for AZ31/AZ91/1.5 vol%Al_2O_3 compared to monolithic AZ31/AZ91 as shown in Fig. 4b. The tensile/compressive strength increase in AZ31/AZ91/1.5 vol%Al_2O_3 compared to monolithic AZ31/AZ91 can be attributed to the following well known factors (pertaining to reinforcement): (a) dislocation generation due to elastic modulus mismatch and coefficient of thermal expansion mismatch between the matrix and reinforcement [22,23,25,26], (b) Orowan strengthening mechanism [25–27] and (c) load transfer from matrix to reinforcement [22,25].

The tensile strength of AZ31/AZ91/1.5 vol%Al_2O_3 was similar to or better than: (a) selected wrought/cast Zr-free (or Al-containing) Mg alloys having similar or higher Al content, (b) selected wrought/cast Zr-containing (or Al-free) Mg alloys, (c) selected wrought Mg nanocomposites (extruded at lower temperature) and (d) selected wrought Zr-free (or Al-containing) Mg alloy microcomposites having higher Al content, as listed in Table 3 [14,28–31]. The compressive strength of AZ31/AZ91/1.5 vol%Al_2O_3 was similar to or better than: (a) selected wrought/cast Zr-free (or Al-containing) Mg alloys having similar or higher Al content, (b) selected cast

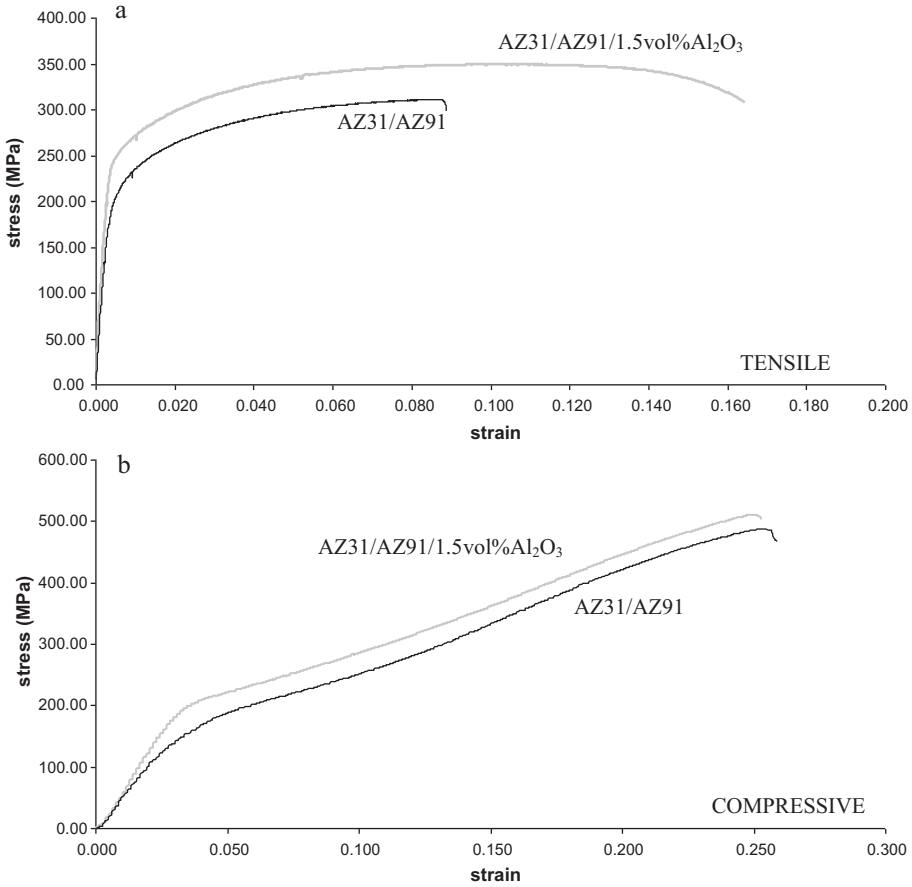

Fig. 4. Representative room temperature: (a) tensile and (b) compressive stress–strain curves of monolithic AZ31/AZ91 and AZ31/AZ91/Al_2O_3 nanocomposite. Tensile and compressive strain rates are 0.01 min^{-1} and 0.005 min^{-1}, respectively.

Zr-containing (or Al-free) Mg alloys and (c) selected cast Zr-containing (or Al-free) Mg alloy microcomposite, as listed in Table 4 [14,32].

In both AZ31/AZ91/1.5 vol%Al_2O_3 and monolithic AZ31/AZ91, 0.2%TYS was about 1.77 and 1.89 times (almost double) the 0.2%CYS, respectively. Here, the tensile/compressive yield stress anisotropy was despite the crystallographic texture exhibited where $\{1\,0\,1\,-2\}\ \langle 1\,0\,1\,-1\rangle$-type twinning was activated along the c-axis of the HCP unit cell in Fig. 3 with comparatively similar ease in both tension and compression along the c-axis, based on the 45° angle between the c-axis and the vertical axis [33,34]. The tensile/compressive yield stress anisotropy can be attributed generally to half the strain rate used (less strain hardening) in compressive testing compared to tensile testing.

4.3.2.2. Failure strain. The tensile and compressive failure strains of monolithic material and nanocomposite are listed in Tables 3 and 4 (and based on stress–strain curves shown in Fig. 4a and b), respectively. Compared to monolithic material, tensile failure strain was enhanced (+99%) in AZ31/AZ91/1.5 vol%Al_2O_3. Compared to monolithic material, compressive failure strain was lowered (−7%) in AZ31/AZ91/1.5 vol%Al_2O_3. The tensile failure strain increase in AZ31/AZ91/1.5 vol%Al_2O_3 compared to monolithic AZ31/AZ91 can be attributed to the following factor (pertaining to reinforcement): (a) presence and reasonably uniform distribution of ceramic nanoparticles [21,31]. Here, it has been shown in previous studies that the nanoparticles provide sites where cleavage cracks are opened ahead of the advancing crack front. This: (1) dissipates the stress concentration which would otherwise exist at the crack front and (2) alters the local effective stress state from plane strain to plane stress in the neighbourhood of crack tip [21,31]. In comparison of compressive failure strain, factor (a) was played down considering the crack-closing nature of compressive deformation, leading to slightly lowered (−7%) failure strain in AZ31/AZ91/1.5 vol%Al_2O_3.

The tensile failure strain of AZ31/AZ91/1.5 vol%Al_2O_3 was similar to or better than: (a) selected wrought/cast Zr-free (or Al-containing) Mg alloys having similar or higher Al content, (b) selected wrought/cast Zr-containing (or Al-free) Mg alloys, (c) selected wrought Mg nanocomposites (extruded at lower temperature) and (d) selected wrought Zr-free (or Al-containing) Mg alloy microcomposites having higher Al content, as listed in Table 3 [14,28–31]. The compressive failure strain of AZ31/AZ91/1.5 vol%Al_2O_3 was similar to or better than: (a) selected cast Zr-containing (or Al-free) Mg alloys and (b) selected cast Zr-containing (or Al-free) Mg alloy microcomposite, as listed in Table 4 [32]. Tensile fracture behavior of both monolithic material and nanocomposite was mixed (ductile + brittle) as shown in Fig. 5a and b. However, the tensile fractured surface of the nanocomposite had: (a) higher occurrence of smaller dimple-like features and (b) absence of microcracks, compared to that of monolithic material. The tensile cavitation resistance was lower and the microcrack formation resistance was higher in the nanocomposite compared to monolithic material. Compressive fracture behavior of AZ31/AZ91/1.5 vol%Al_2O_3 was relatively similar (similar fracture surface exhibited) compared to monolithic material as shown in Fig. 5c. In this case where the l/d ratio of samples was relatively low ($l/d = 1$) [32], the samples failed in shear and not by buckling as illustrated in recent work [35,36].

4.3.2.3. Work of fracture. The tensile and compressive work of fracture (WOF) of monolithic material and nanocomposite are listed in Tables 3 and 4 (and illustrated in Fig. 4a and b), respectively. WOF quantified the ability of the material to absorb energy up to fracture under load [37]. Compared to monolithic material, tensile WOF

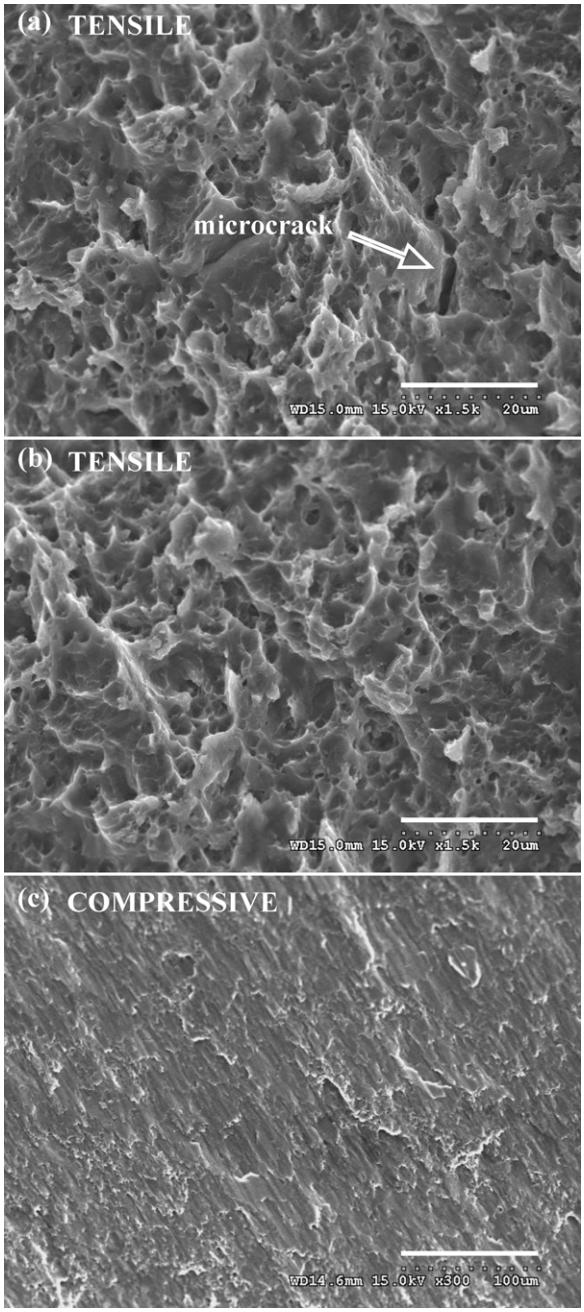

Fig. 5. Representative tensile fractographs of: (a) monolithic AZ31/AZ91 and (b) AZ31/AZ91/Al_2O_3 nanocomposite. (c) Representative compressive fractograph of monolithic AZ31/AZ91 and AZ31/AZ91/Al_2O_3 nanocomposite.

was enhanced (+108%) in AZ31/AZ91/1.5 vol%Al_2O_3. Compared to monolithic material, compressive WOF was decreased (−11%) in AZ31/AZ91/1.5 vol%Al_2O_3. The significantly high increment in tensile WOF and marginal decrement in compressive WOF exhibited by AZ31/AZ91/1.5 vol%Al_2O_3 show its potential to be used in damage tolerant design.

5. Conclusions

Monolithic AZ31/AZ91 and AZ31/AZ91/1.5 vol%Al_2O_3 nanocomposite can be successfully synthesized using the DMD technique followed by hot extrusion.

Compared to monolithic AZ31/AZ91, tensile strength of AZ31/AZ91/1.5 vol%Al_2O_3 was enhanced. Compared to monolithic

AZ31/AZ91, compressive strength of AZ31/AZ91/1.5 vol%Al_2O_3 was increased. This can be attributed to well known factors pertaining to reinforcement.

Compared to monolithic AZ31/AZ91, tensile and compressive failure strain of AZ31/AZ91/1.5 vol%Al_2O_3 was enhanced and decreased, respectively. The increase in failure strain can be attributed to the following factor pertaining to reinforcement: (a) presence and reasonably uniform distribution of Al_2O_3 nanoparticles. This factor was played down considering the crack-closing nature of compressive deformation, leading to slightly lower compressive failure strain in AZ31/AZ91/1.5 vol%Al_2O_3.

Compared to monolithic AZ31/AZ91, AZ31/AZ91/1.5 vol%Al_2O_3 exhibited significantly high increment in tensile WOF and marginal decrement in compressive WOF.

Acknowledgements

Authors wish to acknowledge National University of Singapore (NUS) and Temasek Defence Systems Institute (TDSI) for funding this research (TDSI/09-011/1A and WBS# R265000349).

References

[1] Y. Morisada, H. Fujii, T. Nagaoka, M. Fukusumi, Mater. Sci. Eng. A 433 (2006) 50–54.
[2] Y. Morisada, H. Fujii, T. Nagaoka, M. Fukusumi, Scripta Mater. 55 (2006) 1067–1070.
[3] Y. Morisada, H. Fujii, T. Nagaoka, M. Fukusumi, Mater. Sci. Eng. A 419 (2006) 344–348.
[4] W.B. Ding, H.Y. Jiang, X.Q. Zeng, D.H. Li, S.S. Yao, Appl. Surf. Sci. 253 (2007) 3877–3883.
[5] W. Ding, H. Jiang, X. Zeng, D. Li, S. Yao, Mater. Lett. 61 (2007) 496–501.
[6] D. Wenbin, J. Haiyan, Z. Xiaoqin, L. Dehui, Y. Shoushan, J. Alloys Compd. 429 (2007) 233–241.
[7] Z. Ming-Juan, Z. Long-Zhi, Z. Bing-Feng, Y. Hong, Trans. Nonferrous Met. Soc. China 20 (2010) s476–s480.
[8] C.J. Lee, J.C. Huang, P.J. Hsieh, Scripta Mater. 54 (2006) 1415–1420.
[9] K. Wu, K. Deng, K. Nie, Y. Wu, X. Wang, X. Hu, M. Zheng, Mater. Des. 31 (2010) 3929–3932.
[10] X.J. Wang, X.S. Hu, K. Wu, K.K. Deng, W.M. Gan, C.Y. Wang, M.Y. Zheng, Mater. Sci. Eng. A 492 (2008) 481–485.
[11] C. Badini, M. Ferraris, F. Marchetti, Mater. Lett. 21 (1994) 55–61.
[12] L.M. Tham, M. Gupta, L. Cheng, Mater. Sci. Technol. 15 (1999) 1139–1146.
[13] M. Gupta, M.O. Lai, S.C. Lim, J. Alloys Compd. 260 (1997) 250–255.
[14] M.M. Avedesian, H. Baker, ASM Specialty Handbook: Magnesium and Magnesium Alloys, ASM International®, Ohio, 1999, pp. 12–25, 165–172, 226–248, 258–263.
[15] Q.B. Nguyen, M. Gupta, J. Alloys Compd. 459 (2007) 244–250.
[16] B.Q. Han, D.C. Dunand, Mater. Sci. Eng. A 277 (2000) 297–304.
[17] N. Eustathopoulos, M.G. Nicholas, B. Drevet, Wettability at High Temperatures, Vol. 3, Pergamon Materials Series, Pergamon, New York, 1999.
[18] J.D. Gilchrist, Extraction Metallurgy, third ed., Pergamon Press, New York, 1989.
[19] M. Paramsothy, S.F. Hassan, N. Srikanth, M. Gupta, J. Mater. Sci. 44 (2009) 4860–4873.
[20] M. Gupta, M.O. Lai, C.Y. Soo, Mater. Sci. Eng. A 210 (1996) 114–122.
[21] S.F. Hassan, M. Gupta, J. Alloys Compd. 419 (2006) 84–90.
[22] S.F. Hassan, M. Gupta, J. Mater. Sci. 41 (2006) 2229–2236.
[23] S.F. Hassan, M. Gupta, Metall. Mater. Trans. A 36 (8) (2005) 2253–2258.
[24] C.S. Goh, J. Wei, L.C. Lee, M. Gupta, Nanotechnology 17 (2006) 7–12.
[25] Z. Szaraz, Z. Trojanova, M. Cabbibo, E. Evangelista, Mater. Sci. Eng. A 462 (2007) 225–229.
[26] L.H. Dai, Z. Ling, Y.L. Bai, Comp. Sci. Technol. 61 (2001) 1057–1063.
[27] D. Hull, D.J. Bacon, Introduction to Dislocations, fourth ed., Butterworth-Heinemann, Oxford, 2002, p. 43, 231.
[28] S.F. Hassan, M. Gupta, Comp. Struct. 72 (2006) 19–26.
[29] V. Laurent, P. Jarry, G. Regazzoni, D. Apelian, J. Mater. Sci. 27 (1992) 4447–4459.
[30] A. Tissier, D. Apelian, G. Regazzoni, J. Mater. Sci. 25 (1990) 1184–1196.
[31] S.F. Hassan, M. Gupta, J. Alloys Compd. 429 (2007) 176–183.
[32] D.J. Towle, C.M. Friend, Mater. Sci. Technol. 9 (1993) 35–41.
[33] T. Laser, C. Hartig, M.R. Nurnberg, D. Letzig, R. Bormann, Acta Mater. 56 (2008) 2791–2798.
[34] J. Bohlen, S.B. Yi, J. Swiostek, D. Letzig, H.G. Brokmeier, K.U. Kainer, Scripta Mater. 53 (2005) 259–264.
[35] M. Paramsothy, N. Srikanth, S.F. Hassan, M. Gupta, Mater. Sci. Eng. A 194 (2008) 436–444.
[36] M. Paramsothy, S.F. Hassan, N. Srikanth, M. Gupta, J. Alloys Compd. 482 (2009) 73–80.
[37] R.E. Reed-Hill, Physical Metallurgy Principles, second ed., D Van Nostrand Company, New York, 1964, p. 192, 267, 725.